Atmos. Chem. Phys. Discuss., https://doi.org/10.5194/acp-2018-141
Manuscript under review for journal Atmos. Chem. Phys.
Discussion started: 15 February 2018

Atmospheric Chemistry and Physics
Discussions

Tropical atmospheric circulation response to the G1 sunshade geoengineering radiative forcing experiment

Anboyu Guo[1], John C. Moore[1,2,3], Duoying Ji[1]

[1] College of Global Change and Earth System Science, Beijing Normal University, 19 Xinjiekou Wai St., Beijing, 100875, China

[2] Arctic Centre, University of Lapland, P.O. Box 122, 96101 Rovaniemi, Finland

[3] CAS Center for Excellence in Tibetan Plateau Earth Sciences, Beijing 100101, China

Correspondence to: John C. Moore (john.moore.bnu@gmail.com)

Abstract. We investigate the multi-earth system model response of the Walker circulation and Hadley circulations under the idealized solar radiation management scenario (G1) and under abrupt4×CO_2. The Walker circulation multi-model ensemble mean shows changes in some regions but no significant change in intensity under G1, while it shows 4° eastward movement and 1.9×10^9 kg s^{-1} intensity decrease in abrupt4×CO_2. Variation of the Walker circulation intensity has the same high correlation with sea surface temperature gradient between eastern and western Pacific under both G1 and abrupt4×CO_2. The Hadley circulation shows significant differences in behavior between G1 and abrupt4×CO_2 with intensity reductions in the seasonal maximum northern and southern cells under G1 correlated with equator-ward motion of the Inter Tropical Convergence Zone (ITCZ). Southern and

northern cells have significantly different response, especially under abrupt4×CO_2 when impacts on the southern Ferrel cell are particular clear. The southern cell is about 3% stronger under abrupt4×CO_2 in July, August and September than under piControl, while the northern is reduced by 2% in January, February and March. Both circulations are reduced under G1. There are good correlations between northern cell intensity and land temperatures, but not for the southern cell. Changes in the meridional temperature gradients account for changes in Hadley intensity better than changes in static stability both in G1 and especially in abrupt4×CO_2. The difference in response to the zonal Walker circulation and the meridional Hadley circulations under the idealized forcings may be driven by the zonal symmetric relative cooling of the tropics under G1.

1 Introduction

The large-scale tropical atmospheric circulation may be partitioned into two independent orthogonal overturning convection cells, namely the Hadley circulation (HC) and the Walker circulation (WC), (Schwendike et al., 2014). The Hadley circulation is the zonally symmetric meridional circulation with an ascending branch in the intertropical convergence zone (ITCZ) and a descending branch in the subtropical zone, and which plays a critical role in producing the tropical and subtropical climatic zones, especially deserts (Oort and Yienger, 1996). The Walker circulation is the asymmetric zonal circulation which extends across the entire tropical

Pacific, characterized by an ascending center over the Maritime Continent and western Pacific, eastward moving air flow in the upper troposphere, a strong descending center over the eastern Pacific and surface trade winds blowing counter to the upper winds along the equatorial Pacific completing the circulation (Bjerknes, 1969).

Observational evidence shows a poleward expansion of the Hadley circulation in the past few decades (Hu et al., 2011) and an intensification of the Hadley circulation in the boreal winter (Song and Zhang, 2007). Moreover, climate model simulations with increased greenhouse gas forcing also indicate a poleward expansion of the Hadley circulation, though weaker than that observed (Hu et al., 2013; Ma and Xie, 2013; Kang and Lu, 2012; Davis et al., 2016). Vallis et al. (2015) analysed the response of 40 CMIP5 climate models finding that there was only modest model agreement on changes. Robust results were slight expansion and weakening of the winter cell Hadley circulation in the northern hemisphere. Observational evidence shows a strengthening and westward movement of the Walker circulation from 1979 to 2012 (Bayr et al., 2014; Ma and Zhou, 2016). However, the time required to robustly detect and attribute changes in the tropical Pacific Walker Circulation could be 60 years or more (Tokinaga et al., 2012). Model results suggest a significant eastward movement with weakening intensity under greenhouse gas forcing (Bayr et al., 2014).

Geoengineering as a method of mitigating the deleterious effects anthropogenic climate change has been suggested as a compliment to mitigation and adaptation efforts. For example, Shepherd et al. (2009) summarized the methodologies and governance implications as early as a decade ago. Solar radiation management geoengineering can lessen the effect of global warming due to the increasing concentrations of greenhouse gases by reducing incoming solar radiation. This compensating of longwave radiative forcing with shortwave reductions necessarily leads to non-uniform effects around the globe, as summarized in results for many climate models in the Geoengineering Model Intercomparison Project (GeoMIP) by (Kravitz et al., 2013). This is due to the seasonal and diurnal patterns of short wave forcing being far different from the almost constant long wave radiative absorption. In addition, solar geoengineering, or solar radiation management (SRM), tends to produce net drying due to the change in vertical temperature gradient as greenhouse gasses increase absorption in the troposphere while shortwave radiative forcing affects surface temperatures (Bala et al., 2011). These differences in short and long wave forcing impacts atmospheric circulation and hence precipitation patterns, summarized for the GeoMIP models by Tilmes et al. (2013). There is also a relative undercooling of the polar regions and overcooling of the tropics and a similar response of oceans versus land with globally uniform SRM. Extreme precipitation is affected by SRM such that heavy precipitation events become rarer while small and moderate events become more frequent (Tilmes et al., 2013). This is generally opposite to the impact of greenhouse gas forcing alone which tends to produce a "wet gets wetter and dry gets drier" pattern to global precipitation anomalies (Tilmes et al., 2013). Finally tropical extreme cyclones have been shown to be affected by geoengineering in ways that do not simply reflect changes in tropical sea surface temperatures due to large scale planetary circulations and teleconnection patterns (Moore et al., 2015).

To date, few studies of the impact of geoengineering on tropical atmospheric circulation has been published. Ferraro et al. (2014) using an intermediate complexity climate model found tropical overturning circulation weakens in response to geoengineering with stratospheric sulfate aerosol injection. But geoengineering simulated as a simple reduction in total solar irradiance does not capture this effect. Davis et al. (2016) analyzed 9 GeoMIP models and report that the Hadley circulation expands in response to a quadrupling of atmospheric carbon dioxide concentrations more or less proportionality to the climate sensitivity of the climate model, and shrinks in response to a reduction in solar constant. Smyth et al. (2017) report that changes in the Hadley cells dominate changes in tropical precipitation under solar geoengineering, and that seasonal changes mean that the ITCZ has smaller amplitude migration shifts compared with no geoengineering.

The El Niño Southern Oscillation (ENSO) is the largest mode of multi-annual variability exhibited by the climate system in terms of its temperature variability and also for its socio-economic impacts. This tropical circulation pattern is intimately related to changes in the Walker circulation, and indirectly to the Hadley circulation by its impacts on global energy balance. Few studies of climate model ENSO response to geoengineering have been made, with Gabriel and Robock (2015) finding that stratospheric aerosol injection by the GeoMIP G4 experiment produces no significant impacts on El Niño/Southern Oscillation. The signal to noise ratio in the G4 experiment is relatively low with a background of only the modest RCP4.5 greenhouse gas forcing scenario. However, this topic is worthy or more investigation since one concern is that SRM geoengineering will place the climate system into a new regime of variability (Robock, 2008; Shepherd, 2009). If this were the case then we would expect that the dominant climate modes of variability would also differ from both pre-industrial conditions and those under greenhouse gas forcing alone. Although this can be studied via volcanic analogues, they are imperfect due to their transient nature compared with long-term deployment of geoengineering (Robock et al., 2008). Tropical volcanic eruptions do indeed change the global circulation (Robock, 2000), and so climate mode change is a potential risk of geoengineering. Hence examining the tropical circulation and their response under ENSO modulation can provide evidence on the likelihood of geoengineering inducing a regime change on the global climate system.

In this paper we utilize simulation results from 8 Earth System Models (ESM) that participated in the GeoMIP G1 experiment (Kravitz et al., 2011) and compare these results with the corresponding Climate Model Intercomparison Project Phases 5 (CMIP5) experiment for abrupt quadrupling of CO_2 (abrupt4×CO_2) and preindustrial conditions (piControl). The G1 scenario is the largest geoengineering signal addressed to date by experiments given that it is designed to balance radiative forcing from quadrupled CO_2, hence the signal to noise ratio is high, and furthermore it has been completed a by a large number of ESM and so we can examine across model differences in simulations. We address the following key questions: Does the G1 scenario counteract position and intensity variations in the Walker and Hadley circulations caused by the greenhouse gas long wave forcing under abrupt4×CO_2?; and how does the tropical atmospheric circulation, including the Walker and Hadley circulations, respond to warm and cold phases of the El Niño Southern Oscillation (ENSO) in G1 and abrupt4×CO_2

2 Data and methods

We use 8 ESM (Table 1), a subset of the group described in Kravitz et al. (2013) that have completed G1. We are limited to these models due to unavailability of some fields in the output from other models. The simulations in each model are initiated from a preindustrial conditions which has reached steady state, denoted as piControl, which is the standard CMIP5 name for this experiment (Taylor et al., 2012). Our reference simulation, denoted abrupt4×$CO_{2,}$ is also a standard CMIP5 experiment in which CO_2 concentrations are instantaneously quadrupled from the control run. This experiment implies an atmospheric CO_2 concentration of nearly 1140 ppm, close to "business as usual" scenarios such as RCP8.5 by the year 2100. Experiment G1 in GeoMIP involves an instantaneous reduction of insolation simultaneous with this CO_2

Atmos. Chem. Phys. Discuss., https://doi.org/10.5194/acp-2018-141
Manuscript under review for journal Atmos. Chem. Phys.
Discussion started: 15 February 2018

increase such that top-of-atmosphere (TOA) radiation differences between G1 and piControl are no more than 0.1 W m^{-2} for the first 10 years of the 50 year experiment (Kravitz et al., 2011). The amount of solar radiation reduction is model dependent but does not vary during the course of the simulation.

We used the following variables from 8 climate models and reanalysis data (Table 1): sea level pressure (SLP), sea surface temperature (SST), zonal wind (*U*), meridional wind (*V*) Sea level pressure and sea surface temperature interpolated onto a regular 1°× 1°grid. The zonal and meridional wind are regridded onto a common horizontal fixed grid of 2.5°× 2.5°as in many preceding studies (Bayr et al., 2014; Ma and Zhou, 2016; Stachnik and Schumacher, 2011). All the data we used are monthly-mean model output. Reanalysis data span the years 1979-2016.

Composite analysis is applied for the study on the influence of ENSO. We follow Bayr et al. (2014) and use detrended and normalized Nino3.4 index (monthly averaged sea surface temperature anomaly in the region bounded by 5°N - 5°S, from 170°W - 120°W) as a criteria to select ENSO event. An index > 1 represents an El Niño event and < -1 a La Niña one (Bayr et al., 2014). We concatenate variables in all El Niño and La Niña events for each individual model to get El Niño and La Niña data sets and then calculate ensemble results.

2.1 Mass stream-function

The Hadley and Walker circulations represent the meridional and zonal components of the complete three-dimensional tropical atmospheric circulation. We follow many previous authors (e.g. Davis et al., 2016; Bayr et al., 2014; Nguyen et al., 2013; Ma and Zhou, 2016; Yu et al., 2012) in using mass stream-function to conveniently separate and picture these two convective flows.

The zonal mass stream-function (ψ_z) and meridional mass stream-function (ψ_m) are defined as following:

$$\psi_z = \frac{2\pi a}{g}\int_0^{p_s} u_D dp \qquad (1) \qquad\qquad \psi_m = \frac{2\pi a\cos(\phi)}{g}\int_0^{p_s} v\, dp \qquad (2)$$

where u_D and v respectively represent the divergent component of the zonal wind and the zonal-mean meridional wind, a is the radius of Earth, g is the acceleration of gravity (9.8 ms^{-2}), p is the pressure, p_s is the surface pressure, and the ϕ in (2) is latitude. The meridionally averaged u_D between 5°S and 5°N are integrated from top of the atmosphere to the surface in calculating the zonal mass stream-function (ψ_z).

Some previous studies have removed the fast response transient and only use years 11-50 of G1 and abrupt4×CO_2 to avoid climate transient effects (e.g. Smyth et al., 2017; Kravitz et al., 2013), while Davis et al. (2016) discarded the first 5 years, noting that the choice is conservative. We examine if zonal and meridional mass stream-function have transient effects at the start of the simulation. Fig. S1We shows the time series of the Walker circulation as defined by the vertically averaged value of the stream function ψ_z (STRF, see section 2.2), and shows that there is variability at many timescales up to decadal but without significant transient effects. This is confirmed by statistical analysis of each model; for example there are 4 models (CCSM4, HadGEM2-ES, IPSL-CM5A-LR and MIROC-ESM) that have significantly higher STRF in the first 10 years of the abrupt4×CO_2 simulation than in following decades. But this is not due to a transient affecting the first few years, but rather to higher values around 3 years into the simulation, but this is not unusual for each model's multiannual and decadal variability. On the other hand, the measures of circulation that rely on sea surface temperature (Fig. S2) show some difference in the first decade compared with later periods under abrupt4×CO_2. The Hadley cell vertically averaged stream-function shows similar results and strong seasonal variability (not shown). Therefore to utilize as much data as possible and increase the robustness of our statistical analysis, we use all 50 years of G1 and abrupt4×CO_2 simulations. We use 100 years of piControl simulations as baseline climate for the same reason.

2.2 Walker circulation index

Four related indices have been used to characterize the Walker circulation intensity and its position. Tropical Pacific east-west gradients, defined by conditions in the Darwin region (5°S - 5°N, 80°E - 160°E) and the Tahiti region (5°S - 5°N, 160°W - 80°E) of sea level pressure (ΔSLP) and temperature (ΔSST), (Bayr et al., 2014; DiNezio et al., 2013; Ma and Zhou, 2016; Vecchi and Soden, 2007; Vecchi et al., 2006) are highly correlated for all 3 experiments discussed here with R^2 around 0.9. Ma and Zhou (2016) used the vertically averaged value of the stream function ψ_z (STRF), over the western and central Pacific (150°E – 150°W) and this is also very highly correlated with ΔSST and ΔSLP. As we are interested in the structure of the circulation, so use either the whole stream function, or the STRF in rest of the paper.

To determine the Walker circulation movement in different experiments, we use the western edge of Walker circulation to represent it position. The western edge is defined by the zero value of the vertically averaged ψ_z between 400 – 600 hPa in the western Pacific 120°E – 180°E, (Ma and Zhou, 2016).

2.3 Hadley circulation index

Many authors have separated the northern and southern Hadley circulation cells simply by dividing by hemisphere (e.g., Davis et al., 2016), but during the active periods of each cell, the circulation extends across the equator into the opposite hemisphere. The boundary at the edge of the tropics is also known to change but the circulation cell rapidly becomes weaker beyond the zero crossing of the rotation sense. To capture the variability of the Hadley circulation cells we select the season of maximum intensity for each cell, and measure the strength across its full latitudinal extent. Thus we define the Hadley circulation intensity for the southern cell with the meridional stream-function between 40°S and 15°N in July, August and September (JAS), and the northern cell as the absolute value of mean meridional stream-function between 15°S and 40°N in January, February and March (JFM). We use the 900 – 100 hPa levels (whereas typically 200 hPa has been the ceiling, (e.g., Nguyen et al., 2013)) to accommodate the raised tropopause under greenhouse gas forcing, while avoiding boundary effects.

3 Walker circulation response

3.1 Intensity

The mean state of zonal mass stream-function (ψ_z) calculated from 8 ensemble member mean piControl, ERA-Interim reanalysis and the NCEP2 reanalysis results are shown in Fig. 1. Zonal mass stream-function (ψ_z) can intuitively depict the Walker circulation which exhibits its strongest convection (positive values) in the equatorial zone across the Pacific. The Walker circulation center is around 500hPa and 160°W. Fig. 1 shows that the ensemble piControl circulation has a westward displacement and the intensity measured by STRF is underestimated by 3% relative to ERA-Interim. There is a similar structure to the stream function differences between piControl and NCEP2 reanalysis, but with larger magnitudes than from ERA-Interim.

The relative changes from piControl under G1 and abrupt4×CO_2 experiments are shown in Fig. 2. The features of Walker circulation are very similar in both the G1 and piControl experiments. In abrupt4×CO_2 differences are larger, and include a rise in vertical extent of the circulation and an eastward shift. This is quantifiably confirmed by the STRF index increase of just 0.3% in G1 but a decrease of 7% in abrupt4×CO_2 relative to piControl, (Table 2). The reanalysis data including ERA-Interim and NCEP2 respectively show 7.6×10^{10} kg s^{-1} and 0.7×10^{10} kg s^{-1} stronger intensity. There is much diversity between individual models (Fig. S3).

3.2 Position

The vertically averaged zonal mass stream-function (ψ_z) for the ensemble means of the 3 experiments as a function of longitude are shown in Fig. 3. To quantitatively measure the position change of the Walker circulation we use the western edge index. The ERA-Interim and NCEP2 reanalysis data respectively show 10.5° and 18° more easterly positions than the piControl state. The Walker circulation shifts 0.5° westward in G1 and 4° eastward in abrupt4×CO_2 relative to piControl for the multi-model ensemble mean. However there is some scatter between models (Table 2). In the G1 experiment, the Walker circulation strengthens over the western Pacific around 130°E to 150°E and weakens over the eastern Pacific around 115°W to 80°W, indicating a westward movement relative to piControl, (Table 2). Thus the pattern is the opposite of that seen under abrupt4×CO_2.

Under G1 there is a westward shift in the ascending branch of the circulation from about 30 ° E to about 20 ° E as indicated by comparing the red shaded region around 30°E in Fig. 2 with the piControl result in Fig. 1. Fig. S3 shows the anomaly is present in CanESM2, CCSM4, and NorESM1-M, while 3 models show almost no change (and indeed are missing the African features in their piControl simulation). BNU-ESM shows the opposite anomaly while GISS-E2-R shows a complex pattern. There is only small change in the STRF zero crossing location in the region (Fig. 3) because of the anomalies are not vertical. This position is at the transition from tropical West African rainforest to wood and grassland in East Africa under present climates. The movement westward would impact the rain forests of the Congo basin. There is no similar positional change under abrupt4×CO_2 in the region, though there are many more changes in the circulation as a whole.

4 Hadley circulation intensity response

The climatology of the meridional mass stream-function (ψ_m) calculated from multi-model ensemble mean are shown in Figs. 4 and 5 and the individual models are shown in Fig. S4. This can intuitive describe the Hadley circulation with a clockwise rotation in the northern hemisphere and an anticlockwise rotation in the southern hemisphere. The southern Hadley cell width spans nearly 35°of latitude and the northern Hadley cell about 25° latitude. The intensity anomalies relative to piControl from both the reanalysis data sets are less than 19% (Fig. 4).

Circulation anomalies under abrupt4×CO_2 (Fig. 5), show increased poleward flow at upper levels of the troposphere and decreased equatorial flow at lower levels in both northern and southern Hadley cells. The elevation of the circulation upper branches rises with increased greenhouse gas concentration, as previously noted (Vallis et al., 2015), and is likely a consequence of the rise in tropopause height due to greenhouse gases. The southern cell shows a complex anomaly structure with large changes also in the Ferrel cell circulation that borders it at higher southern latitudes. The northern cell anomaly is simple in comparison. Under G1 the changes are largest near the equatorial margins of the cells, with a clear increase in the strength of the ascending current. There is no significant change in the upper branch of the circulation showing that the tropopause is returned to close to piControl conditions despite the greenhouse concentrations being raised. Seasonal differences illustrate the changes induced under the experiments in a clearer way than the annual ensemble result (Fig. 6).

In JAS, when the ITCZ is located furthest north around 15°N, the G1 anomaly indicates a reduction in the upward branch of the southern cell, or equivalently, a southern migration of the ITCZ. Similarly in JFM there is a corresponding reduction in strength of the upwelling branch of the northern cell (Fig. 6). This is a similar result as obtained by Smyth et al. (2017) who considered the ITCZ position to be defined as the centroid of precipitation, and found changes in position of fractions of a degree. Fig. 7 shows that there is a good relationship between the intensity of the southern cell peak intensity with the motion of the ITCZ, showing that the larger the model reduction in intensity the more the boundary of the ITCZ moves equatorward. The correlation for the northern cell is not strong to be significant though still indicates correlation between intensity and ITCZ position changes. The combined seasonal effect of both cell changes is a reduced migration of the upwelling branches of the circulation cells across the equator.

The GISS-E2-R model has strikingly different anomalies under both G1 and abrupt4×CO_2 compared with other models, with much more variability and more changes in sign of rotation not only within the Hadley cell but in the surrounding Ferrel cells. If we exclude this model from the ensemble, we get an even clearer result showing that the movement of the equatorial edge of the Hadley cells (the ITCZ) totally dominates the response under G1 (Fig. S5).

The situation under abrupt4×CO_2 is more complex. There is an increase in poleward circulation in the upper troposphere in Fig. 5. Similarly there is decrease in equatorward lower tropospheric flow, though it is apparent that the northern cell changes are simpler than those in the southern one. Since there is more mass at lower altitudes the net result is weakening of the circulation cells. The expansion poleward of the cells can be seen by the blue shading in the lower troposphere around 30°S in JAS and corresponding red shading around 30°N in JFM. The expansion of the tropics has been noted both in greenhouse gas simulations and observationally (Davis et al., 2016; Hu et al., 2011). It is noticeable that the southern expansion appears greater than the northern one, as was also deduced by Davis et al. (2016) based on the location of the zero in the vertically integrated stream-function. It is also clear that the extratropical changes in the Ferrel circulation are more pronounced in the southern hemisphere than the northern one.

We use the magnitude of the mean southern Hadley cell intensity (as defined in Section 2.3) during JAS and of northern Hadley intensity during JFM to represent the model behavior under each climate scenario, and plot differences relative to piControl in Fig. 8. The multi-model ensemble mean reveals a diminished northern Hadley intensity under G1 of -18×10^{8} kg s^{-1} and of -7×10^{8} kg s^{-1} for abrupt4×CO_2. The southern Hadley intensity in JAS exhibits a fall of -16×10^{8} kg s^{-1} under G1 but an increase of 23×10^{8} kg s^{-1} under abrupt4×CO_2. The anomalies for most models are significant, and the ensemble means are hugely significant. The reduction in strength of the northern hemisphere winter cell was also a robust result of climate models under RCP8.5, while, in contrast to our Fig. 8 result, the southern cell exhibited almost no change (Vallis et al., 2015).

5 ENSO variability of Walker and Hadley circulations

Many previous study have concluded that the Walker circulation weakens and shifts eastward during El Niño, with opposite effects under La Niña, (Ma and Zhou, 2016; Power and Kociuba, 2011; Yu et al., 2012; Power and Smith, 2007). While the Hadley circulation shrinks and strengthens during El Niño and oppositely under La Niña, (Nguyen et al., 2013; Stachnik and Schumacher, 2011). The G1 solar dimming geoengineering impacts on the Walker and Hadley circulation during ENSO events will be discussed in this section.

The Walker circulation difference between G1, abrupt4×CO_2 and piControl vary among models during ENSO events (Fig. S6). But the multi-model ensemble mean presents a clear picture (Fig. 9). The result show that features of Walker circulation response to ENSO are significantly changed under abrupt4×CO_2 compared with piControl, while G1 compares quite closely to piControl. Differences between G1 and piControl only manifest themselves at the eastern (about 165°E-180°E) and western (about 120°W-90°W) sides of Walker circulation, with a significant westward movement during El Niño, and no significant changes during La Niña.

In contrast under abrupt4×CO_2 almost the whole Walker circulation (about 165°E-105°W) strengthens in intensity and the western edge shifts westward at the 95% statistical significance level during El Niño relative to piControl. During La Niña there is a significant eastward movement in general.

Hadley circulation responses to ENSO under G1, abrupt4×CO_2 and piControl vary among models (Fig. S7). Fig. 10 shows the ensemble mean results. As with the Walker circulation, the climatological features of the Hadley cell show more significant changes under abrupt4×CO_2 than G1 compared with piControl.

The most notable feature of Fig. 10 is the increase in intensity during La Niña between 10°S and 10°N under abrupt4×CO_2. This corresponds to changes in the southern Hadley cell (remembering that the axis of the Hadley cells is northwards of the equator). Also under the same conditions there is weakening of the northern

Hadley cell between 10°and 20°N. The same features are almost as noticeable for abrupt4×CO_2 for El Niño conditions and hence is a general feature of the abrupt4×CO_2 climate state. Beyond the Hadley cells there are modest, but statistically significant changes in the Ferrel circulations, particularly in the Southern hemisphere. Changes under G1 in comparison are much smaller than under abrupt4×CO_2, though there are significant reductions in intensity near the margins of the Hadley cells. The northern cell is more affected in El Niño, while the southern one more in La Niña states.

6 Hadley and Walker circulations relationships with temperature

6.1 Walker Circulation

Changes in tropical Pacific SST dominate the global warming response of the Walker circulation change (Sandeep et al., 2014). A reduced SST gradient between eastern and western Pacific drives the weakening of Walker circulation that was seen in a quadrupled CO_2 experiment (Knutson and Manabe, 1995). The temperature difference between eastern and western Pacific, △SST, explains 96% of the inter-model variance in the strength of the Walker circulation in the G1-piControl anomalies and 79% of the variance for abrupt4×CO_2-piControl, (Fig. 11). There is no difference in model behavior between the G1 and abrupt4×CO_2 anomalies and △SST explains 83% of the overall variance. Despite a temperature transient of at a decade or so (e.g. Kravitz et al., 2013) in the abrupt4×CO_2 simulation and the lack of any

Atmos. Chem. Phys. Discuss., https://doi.org/10.5194/acp-2018-141
Manuscript under review for journal Atmos. Chem. Phys.
Discussion started: 15 February 2018

transient in STRF (Fig. S1), the relationship with ΔSST is nearly as good as for piControl. This suggests that there is no difference in mode of behavior of the Walker circulation under solar dimming geoengineering or greenhouse gas forcing, in contrast with the changes seen in the Hadley cells.

Some models have strong correlation between monthly temperature and Walker circulation (not shown), with positive correlation in northern hemisphere and negative correlation in southern hemisphere due to those models having strong seasonality in their STRF (Fig. S1). The correlation between yearly STRF and global 2 m temperatures are shown in Fig. 12 and the individual models are shown in Fig. S8. We discard first 20 years for G1 and abrupt4×CO_2 to remove the temperature transients. In G1 all models except CanESM2 and MIROC-ESM have strong negative correlations between STRF and tropical Pacific temperatures. BNU-ESM, CCSM4 and NorESM1-M show a positive correlation with temperatures in the South Pacific convergence zone (SPCZ) and its linear extension in the South Atlantic. These features are generally muted or absent in the piControl simulations. Experiments suggest that a key feature of the diagonal structure of the SPCZ is the zonal temperature gradient in the Pacific which allows warm moist air from the equator into the SPCZ region. This moisture then intensifies (diagonal) bands of convection carried by Rossby waves (Van der Wiel et al., 2016). The three models with the positive correlation between STRF and SPCZ temperatures except BNU-ESM have increased STRF and ΔSST under G1 (Fig. 11) suggesting that this mechanism is

Atmos. Chem. Phys. Discuss., https://doi.org/10.5194/acp-2018-141
Manuscript under review for journal Atmos. Chem. Phys.
Discussion started: 15 February 2018

Atmospheric Chemistry and Physics Discussions

responsive in at least some of the models to G1 changes in forcing. The SPCZ is the only part of the ITCZ that extends beyond the tropics and so may be expected to be more subject to the meridional gradients in radiative forcing produced by G1. The correlations under abrupt4×CO_2 are more variable across the models, though some of models like IPSL-CM5A-LR, MIROC-ESM and HadGEM2-ES exhibit widespread anti-correlation between STRF and temperatures; the spatial variability suggests that this not due to the strong transient response in global temperature rises under abrupt4×CO_2.

6.2 Hadley Circulation

We now consider how surface temperature changes may impact the Hadley circulation. To remove the transients, we only use the last 30 years for G1 and abrupt4×CO_2. The decrease of the northern Hadley cell intensity in JFM (Fig. 8) correlates with northern hemispheric land temperatures (Fig. 13), explaining 58% of the variance in model anomaly under G1 – which is nevertheless not significant at the 95% level - and 81% under abrupt4×CO_2. Northern hemisphere land temperature also explains 83% of the G1 anomaly in the southern Hadley cell in JAS, but has no impact on the abrupt4×CO_2 anomaly. We explored the impact of land-ocean temperature differences by considering the Tibet and tropical ocean temperature differences (Fig. S9). Results were similar as for Fig. 13, with significant correlations for G1 in the southern Hadley cell.

Seo et al. (2014) examine the relative importance of changes in meridional temperature gradients in potential temperature, subtropical tropopause height, and static stability on the strength of the Hadley circulation. They find that according to both scaling theory based on the Held and Hou (1980) and the Held (2000) models, and analysis of 30 CMIP5 models forced by the RCP8.5 scenario, that it is the meridional temperature gradient that is the most important factor.

We used the same procedure atsSeo et al. (2014) on the 4 models (BNU-ESM, IPSL-CM5A-LR, HadGEM2-ES, MIROC-ESM) that provide all the fields needed under G1 and abrupt4×CO2 scenarios (Table 3). The changes in ensemble mean circulation intensity are similar under G1 and abrupt4×CO2, as are the changes in potential temperature gradients relative to piControl, but the changes in static stability are very different between the experiments. The tropospheric heights also change between G1 and abrupt4×CO2 scenarios, with small reductions under G1 and about a 3% and 0.9% increase respectively in south and north cell under abrupt4×CO2. We used the two scaling relations given by Seo et al., (2014) to also estimate the change in Hadley intensity based on the changes in temperature gradients, static stability and tropospheric height for the ensemble mean of the 4 models (Table 3). Both formulations give fairly similar numbers for the estimated change in Hadley intensities in northern and southern cells under G1 and abrupt4×CO2. These estimates agree with the simulated changes in intensities under G1, but are very different from those simulated under abrupt4×CO2. The obvious cause of the discrepancies under abrupt4×CO2 is the change in static stability, which in both model scaling formulations leads to 18-25% reductions in Hadley intensity compared with the ensemble model simulated changes of about ±4%. This supports the analysis of Seo et al. (2014) that it is the meridional temperature gradient that is the dominant factor in determining the strength of the Hadley circulation.

7 Discussion

Our main purpose in this study has been to analyze the response of Walker and Hadley circulation to greenhouse gas and solar dimming geoengineering forcing simulated by abrupt4×CO_2 and G1 experiments. A clear Walker circulation westward movement during El Niño and an eastward movement during La Niña are shown nearly everywhere along the equator in abrupt4×CO_2 relative to piControl. However only the eastern and western side of Walker circulation manifest the same movement during ENSO events in G1 relative to piControl. The range and amplitudes of significant changes are smaller in G1 than in abrupt4×CO_2. We note a potentially important change in position of the walker Circulation associated with the West African rainforest and East African grassland zones, under G1, with potential for the encroachment of a drier climate into the Congo basin.

Davis et al., (2016) note an expansion in the Hadley cells in proportion to the temperature rises in the models under both G1 and abrupt4×CO_2. Here, we see large changes throughout the whole Hadley cell circulation under abrupt4×CO_2. We also see that the northern boundary of the Southern cell tends to expand even further northwards with a corresponding weakening of the northern cell during La Niña conditions. Global temperatures are relatively reduced during La Niña years. Beyond the Hadley cells there are modest, but statistically significant changes, in the Ferrel circulations, particularly in the Southern hemisphere. Changes under G1 in comparison are much smaller than under abrupt4×CO_2, though there are significant reductions in intensity near the margins of the Hadley cells and these are related to equator-ward motion of the ITCZ. The northern cell is affected more in El Niño, while the southern one more by La Niña states.

Davis et al. (2016) show that southern Hadley cell expansion in the tropics is on average twice the northern Hadley expansion. The idealized forcings in abrupt4×CO_2 and G1 show this cannot be due to stratosphere ozone depletion – the mechanism sometimes used to account for the similar observed greater expansion of the southern Hadley cell (Waugh et al., 2015). The changes in width of the tropical belt is strongly dependent on the tropical static stability in the models according to the Held and Hou (1980) scaling, that is with the potential temperatures at the tropical tropopause (100 hPa) and the surface. Since the adiabatic lapse rates scales with surface temperature, this is also reflected in the surface temperature. Consideration of simplified convective systems based on moist static energy fluxes (Davis, 2017), or by making some assumptions with the Held (2000) and Held and Hou (1980) models led Seo et al. (2014) to suggest Hadley cell intensity scales according to the equator-pole temperature gradient.

Furthermore the intensity of the Hadley circulation is expected to decrease as it expands and also in response to an accelerated hydrological cycle – that is expected under greenhouse gas forcing, but not solar geoengineering which leads to net drying (Kravitz et al., 2013). This is cannot be a complete explanation for circulation changes since the Hadley circulation also depends on the evolution of the baroclinic instabilities in the extratropics, which may have quite different response to climate warming (e.g. Vallis et al., 2015). Our analysis of intensity shows differences in behavior between southern and northern cells, and in particular a lack of a strong dependences on temperature gradients for the southern cell. The difference in behavior between northern and southern Hadley cells has not been explained to date. Seo et al. (2014) note that under RCP8.5 forcing, models of the southern Hadley cell changes are split almost equally between those predicting increases in intensity and those that suggest decreases, whereas all but 1 of 30 models predicts a decrease in the northern cell. We note that the vertical expansion of the circulation under abrupt4×CO_2, has been associated with an expected decrease in the circulation. But we observe an increase in the southern Hadley cell intensity, while the northern one is stronger than under the G1 forcing. Our analysis of the relative importance of factors in driving intensity suggests, as with Seo et al (2014), that the meridional temperature gradient plays the dominant role rather than tropopause height or static stability changes.

The response times of the Hadley circulations to changes in radiative forcing are very fast, as shown by the lack of transients in the simulated time series. Surface temperature, especially under the strong abrupt4×CO_2 forcing takes at least a decade and parts of the system, such as the ocean and ice, would require even longer to reach equilibrium. The northern hemisphere continents have faster response times than the oceans and so we would expect the southern hemisphere to perhaps be much further from an equilibrium response than the northern one. This is also reflected in the lack of an equivalent to the "Arctic amplification" seen in the northern hemisphere under both observed and simulated forcing by greenhouse gases. The lack of anomalous southern polar warming is linked to the much cooler surface temperatures in the Antarctic mitigating against both temperature feedbacks and the ice-albedo feedback mechanism (Pithan and Mauritsen, 2014).

Our analysis of circulation intensity changes and their dependence on temperature changes shows quite different sets of behavior under G1 than under abrupt4×CO_2 for the Hadley but not the Walker circulation. The response under G1 relative to piControl is a slight overcooling of the tropics relative to the global mean temperature (Kravitz et al., 2013). Experiments with idealized climate models (Tandon et al., 2013) show that heating at the equator alone tends to reduce the Hadley cell width, while wider heating in an annulus around the outer tropics (20°-35°) tends to produce a complex response to circulation in both Hadley and Ferrel cells, more reminiscent of the anomaly patterns seen under abrupt4×CO_2. The climate forcing under G1 is designed to be zonally symmetric, and that may explain lack of impact in the Walker circulation

Atmos. Chem. Phys. Discuss., https://doi.org/10.5194/acp-2018-141
Manuscript under review for journal Atmos. Chem. Phys.
Discussion started: 15 February 2018

Atmospheric Chemistry and Physics Open Access Discussions EGU

under both G1 and greenhouse gas forcing. While under the latitudinal varying forcing of G1 there are clear changes in the Hadley cell. The reduction in incoming shortwave radiation in G1 would intuitively mean reduced heating and moisture flux in the ITCZ, which follows the movement of the sun. Reduced ocean heating would then tend to mean a smaller amplitude of seasonal movement of the ITCZ. Analysis of extreme precipitation events in daily data from the GeoMIP models (Ji et al., submitted to ACP) shows that the frequency of the Rx5day extreme is decreased under G1 along a seasonal path that follows the ITCZ motion, while precipitation extremes increase in the tropical dry seasons. This result is consistent with the variation in the Hadley intensity cell seen here.

Both models and the limited observational data available on the Hadley circulation indicate that it is not zonally symmetric: there are intense regions at the eastern sides of the oceanic basins (Amaya et al., 2017), and much of the natural variability of the circulation is related to ENSO. This and the opposite correlations with surface temperatures in the Pacific and SPCZ with STRF under G1 (Fig. 12) suggests an interplay between Hadley and Walker circulations that could repay further consideration of model data at seasonal scales. The importance of the tropical ocean basins as genesis regions for intense storms also suggests that changed radiative forcing there under geoengineering could cause important differences in seasonal precipitation extremes, that maybe hidden in monthly or annual datasets.

Acknowledgements. We thank the climate modeling groups for participating in the Geoengineering Model Intercomparison Project and their model development teams; the CLIVAR/WCRP Working Group on Coupled Modeling for endorsing the GeoMIP; and the scientists managing the earth system grid data nodes who have assisted with making GeoMIP output available. This research was funded by the National Basic Research Program of China (Grant 2015CB953600).

References

Amaya, D. J., Siler, N., Xie, S.-P., and Miller, A. J.: The interplay of internal and forced modes of Hadley Cell expansion: lessons from the global warming hiatus, Clim Dynam, 1-15, 2017.

Arora, V. K., Scinocca, J. F., Boer, G. J., Christian, J. R., Denman, K. L., Flato, G. M., Kharin, V. V., Lee, W. G., and Merryfield, W. J.: Carbon emission limits required to satisfy future representative concentration pathways of greenhouse gases, Geophys Res Lett, 38, 2011.

Bala, G., Caldeira, K., Nemani, R., Cao, L., Ban-Weiss, G., and Shin, H. J.: Albedo enhancement of marine clouds to counteract global warming: impacts on the hydrological cycle, Clim Dynam, 37, 915-931, 2011.

Bayr, T., Dommenget, D., Martin, T., and Power, S. B.: The eastward shift of the Walker Circulation in response to global warming and its relationship to ENSO variability, Clim Dynam, 43, 2747-2763, 2014.

Bentsen, M., Bethke, I., Debernard, J. B., Iversen, T., Kirkevag, A., Seland, O., Drange, H., Roelandt, C., Seierstad, I. A., Hoose, C., and Kristjansson, J. E.: The Norwegian Earth System Model, NorESM1-M - Part 1: Description and basic evaluation of the physical climate, Geosci Model Dev, 6, 687-720, 2013.

Bjerknes, J.: Atmospheric teleconnections from the equatorial, 1969.

Collins, W. J., Bellouin, N., Doutriaux-Boucher, M., Gedney, N., Halloran, P., Hinton, T., Hughes, J., Jones, C. D., Joshi, M., Liddicoat, S., Martin, G., O'Connor, F., Rae, J., Senior, C., Sitch, S., Totterdell, I., Wiltshire, A., and Woodward, S.: Development and evaluation of an Earth-System model-HadGEM2, Geosci Model Dev, 4, 1051-1075, 2011.

Davis, N. A., Seidel, D. J., Birner, T., Davis, S. M., and Tilmes, S.: Changes in the width of the tropical belt due to simple radiative forcing changes in the GeoMIP simulations, Atmos Chem Phys, 16, 10083-10095, 10.5194/acp-16-10083-2016, 2016.

Davis, N. A.: The Dynamics of Hadley Circulation Variability and Change, Colorado State University. Libraries, 2017.

DiNezio, P. N., Vecchi, G. A., and Clement, A. C.: Detectability of Changes in the Walker Circulation in Response to Global Warming, J Climate, 26, 4038-4048, 2013.

Dufresne, J. L., Foujols, M. A., Denvil, S., Caubel, A., Marti, O., Aumont, O., Balkanski, Y., Bekki, S., Bellenger, H., Benshila, R., Bony, S., Bopp, L., Braconnot, P., Brockmann, P., Cadule, P., Cheruy, F., Codron, F., Cozic, A., Cugnet, D., de Noblet, N., Duvel, J. P., Ethe, C., Fairhead, L., Fichefet, T., Flavoni, S., Friedlingstein, P., Grandpeix, J. Y., Guez, L., Guilyardi, E., Hauglustaine, D., Hourdin, F., Idelkadi, A., Ghattas, J., Joussaume, S., Kageyama, M., Krinner, G., Labetoulle, S., Lahellec, A., Lefebvre, M. P., Lefevre, F., Levy, C., Li, Z. X., Lloyd, J., Lott, F., Madec, G., Mancip, M., Marchand, M., Masson, S., Meurdesoif, Y., Mignot, J., Musat, I., Parouty, S., Polcher, J., Rio, C., Schulz, M., Swingedouw, D., Szopa, S., Talandier, C., Terray, P., Viovy, N., and Vuichard, N.: Climate change projections using the IPSL-CM5 Earth System Model: from CMIP3 to CMIP5, Clim Dynam, 40, 2123-2165, 2013.

Ferraro, A. J., Highwood, E. J., and Charlton-Perez, A. J.: Weakened tropical circulation and reduced precipitation in response to geoengineering, Environmental Research Letters, 9, 014001, 10.1088/1748-9326/9/1/014001, 2014.

Gabriel, C. J., and Robock, A.: Stratospheric geoengineering impacts on El Nino/Southern Oscillation, Atmos Chem Phys, 15, 11949-11966, 2015.

Gent, P. R., Danabasoglu, G., Donner, L. J., Holland, M. M., Hunke, E. C., Jayne, S. R., Lawrence, D. M., Neale, R. B., Rasch, P. J., Vertenstein, M., Worley, P. H., Yang, Z. L., and Zhang, M. H.: The Community Climate System Model Version 4, J Climate, 24, 4973-4991, 2011.

Atmos. Chem. Phys. Discuss., https://doi.org/10.5194/acp-2018-141
Manuscript under review for journal Atmos. Chem. Phys.
Discussion started: 15 February 2018

Held, I. M.: The general circulation of the atmosphere, in: 2000 Program in Geophysical Fluid Dynamics Proceedings, Woods Hole Oceanographic Institude, Woods Hole, 30-36, 2000.

Held, I. M., and A. Y. Hou: Nonlinear axially symmetric circulations in a nearly inviscid atmosphere, J. Atmos. Sci., 37, 515–533,1980.

Hu, Y. Y., Zhou, C., and Liu, J. P.: Observational Evidence for Poleward Expansion of the Hadley Circulation, Adv Atmos Sci, 28, 33-44, 2011.

Hu, Y. Y., Tao, L. J., and Liu, J. P.: Poleward expansion of the hadley circulation in CMIP5 simulations, Adv Atmos Sci, 30, 790-795, 2013.

Iversen, T., Bentsen, M., Bethke, I., Debernard, J. B., Kirkevag, A., Seland, O., Drange, H., Kristjansson, J. E., Medhaug, I., Sand, M., and Seierstad, I. A.: The Norwegian Earth System Model, NorESM1-M - Part 2: Climate response and scenario projections, Geosci Model Dev, 6, 389-415, 2013.

Ji, D., Wang, L., Feng, J., Wu, Q., Cheng, H., Zhang, Q., Yang, J., Dong, W., Dai, Y., Gong, D., Zhang, R. H., Wang, X., Liu, J., Moore, J. C., Chen, D., and Zhou, M.: Description and basic evaluation of Beijing Normal University Earth System Model (BNU-ESM) version 1, Geosci Model Dev, 7, 2039-2064, 2014.

Ji, D. Fang, F. Curry, C.L., Kashimura, H., Watanabe, S. Cole, J.N.S., Lenton, A., Muri, H., Kravitz, B. and Moore, J.C.: Impacts of solar dimming and stratospheric aerosol geoengineering on extreme temperature and precipitation, Atmos. Chem.

Phys. Disc (in review).

Kanamitsu, M., Ebisuzaki, W., Woollen, J., Yang, S. K., Hnilo, J. J., Fiorino, M., and Potter, G. L.: Ncep-Doe Amip-Ii Reanalysis (R-2), B Am Meteorol Soc, 83, 1631-1643, 2002.

Kang, S. M., and Lu, J.: Expansion of the Hadley Cell under Global Warming: Winter versus Summer, J Climate, 25, 8387-8393, 2012.

Knutson, T. R., and Manabe, S.: Time-Mean Response over the Tropical Pacific to Increased Co2 in a Coupled Ocean-Atmosphere Model, J Climate, 8, 2181-2199, 1995.

Kravitz, B., Robock, A., Boucher, O., Schmidt, H., Taylor, K. E., Stenchikov, G., and Schulz, M.: The Geoengineering Model Intercomparison Project (GeoMIP), Atmospheric Science Letters, 12, 162-167, 10.1002/asl.316, 2011.

Kravitz, B., Caldeira, K., Boucher, O., Robock, A., Rasch, P. J., Alterskjaer, K., Karam, D. B., Cole, J. N. S., Curry, C. L., Haywood, J. M., Irvine, P. J., Ji, D., Jones, A., Kristjánsson, J. E., Lunt, D. J., Moore, J. C., Niemeier, U., Schmidt, H., Schulz, M., Singh, B., Tilmes, S., Watanabe, S., Yang, S., and Yoon, J.-H.: Climate model response from the Geoengineering Model Intercomparison Project (GeoMIP), Journal of Geophysical Research: Atmospheres, 118, 8320-8332, 10.1002/jgrd.50646, 2013.

Ma, J., and Xie, S. P.: Regional Patterns of Sea Surface Temperature Change: A

Atmos. Chem. Phys. Discuss., https://doi.org/10.5194/acp-2018-141
Manuscript under review for journal Atmos. Chem. Phys.
Discussion started: 15 February 2018

Source of Uncertainty in Future Projections of Precipitation and Atmospheric Circulation, J Climate, 26, 2482-2501, 2013.

Ma, S. M., and Zhou, T. J.: Robust Strengthening and Westward Shift of the Tropical Pacific Walker Circulation during 1979-2012: A Comparison of 7 Sets of Reanalysis Data and 26 CMIP5 Models, J Climate, 29, 3097-3118, 2016.

Moore, J. C., Grinsted, A., Guo, X. R., Yu, X. Y., Jevrejeva, S., Rinke, A., Cui, X. F., Kravitz, B., Lenton, A., Watanabe, S., and Ji, D. Y.: Atlantic hurricane surge response to geoengineering, P Natl Acad Sci USA, 112, 13794-13799, 2015.

Nguyen, H., Evans, A., Lucas, C., Smith, I., and Timbal, B.: The Hadley Circulation in Reanalyses: Climatology, Variability, and Change, J Climate, 26, 3357-3376, 10.1175/jcli-d-12-00224.1, 2013.

Oort, A. H., and Yienger, J. J.: Observed interannual variability in the Hadley circulation and its connection to ENSO, J Climate, 9, 2751-2767, 1996.

Pithan, F. and Mauritsen, T.: Arctic amplification dominated by temperature feedbacks in contemporary climate models , Nature Geoscience, 7 (3), pp. 181-184 . doi: 10.1038/ngeo2071, 2014

Robock, A.: Volcanic eruptions and climate, Rev Geophys, 38, 191-219, 2000.

Robock, A.: 20 reasons why geoengineering may be a bad idea, Bulletin of the Atomic Scientists, 64, 14-18, 2008.

Robock, A., Oman, L., and Stenchikov, G. L.: Regional climate responses to

Atmos. Chem. Phys. Discuss., https://doi.org/10.5194/acp-2018-141
Manuscript under review for journal Atmos. Chem. Phys.
Discussion started: 15 February 2018

geoengineering with tropical and Arctic SO2 injections, J Geophys Res-Atmos, 113, 2008.

Sandeep, S., Stordal, F., Sardeshmukh, P. D., and Compo, G. P.: Pacific Walker Circulation variability in coupled and uncoupled climate models, Clim Dynam, 43, 103-117, 2014.

Schmidt, G. A., Kelley, M., Nazarenko, L., Ruedy, R., Russell, G. L., Aleinov, I., Bauer, M., Bauer, S. E., Bhat, M. K., Bleck, R., Canuto, V., Chen, Y. H., Cheng, Y., Clune, T. L., Del Genio, A., de Fainchtein, R., Faluvegi, G., Hansen, J. E., Healy, R. J., Kiang, N. Y., Koch, D., Lacis, A. A., LeGrande, A. N., Lerner, J., Lo, K. K., Matthews, E. E., Menon, S., Miller, R. L., Oinas, V., Oloso, A. O., Perlwitz, J. P., Puma, M. J., Putman, W. M., Rind, D., Romanou, A., Sato, M., Shindell, D. T., Sun, S., Syed, R. A., Tausnev, N., Tsigaridis, K., Unger, N., Voulgarakis, A., Yao, M. S., and Zhang, J. L.: Configuration and assessment of the GISS ModelE2 contributions to the CMIP5 archive, J Adv Model Earth Sy, 6, 141-184, 2014.

Schwendike, J., Govekar, P., Reeder, M. J., Wardle, R., Berry, G. J., and Jakob, C.: Local partitioning of the overturning circulation in the tropics and the connection to the Hadley andWalker circulations, J Geophys Res-Atmos, 119, 1322-1339, 2014.

Seo, K. H., Frierson, D. M. W., and Son, J. H.: A mechanism for future changes in Hadley circulation strength in CMIP5 climate change simulations, Geophys Res Lett, 41, 5251-5258, 2014.

Shepherd, J. G.: Geoengineering the climate: science, governance and uncertainty, Royal Society, 2009.

Simmons, A., Uppala S D, Dee D. D., and Kobayashi, S.: ERA-Interim: new ECMWF reanalysis products from 1989 onwards. ECMWF Newsletter, No. 110, ECMWF, Reading, United Kingdom, 25-35, 2007.

Smyth, J. E., Russotto, R. D., and Storelvmo, T.: Thermodynamic and dynamic responses of the hydrological cycle to solar dimming, Atmos Chem Phys, 17, 6439-6453, 2017.

Song, H., and Zhang, M. H.: Changes of the boreal winter Hadley circulation in the NCEP-NCAR and ECMWF reanalyses: A comparative study, J Climate, 20, 5191-5200, 2007.

Stachnik, J. P., and Schumacher, C.: A comparison of the Hadley circulation in modern reanalyses, Journal of Geophysical Research: Atmospheres, 116, n/a-n/a, 10.1029/2011jd016677, 2011.

Tandon, N. F., Gerber, E. P., Sobel, A. H., and Polvani, L. M.: Understanding Hadley Cell Expansion versus Contraction: Insights from Simplified Models and Implications for Recent Observations, J Climate, 26, 4304-4321, 2013.

Taylor, K. E., Stouffer, R. J., and Meehl, G. A.: An Overview of Cmip5 and the Experiment Design, B Am Meteorol Soc, 93, 485-498, 2012.

Tilmes, S., Fasullo, J., Lamarque, J.-F., Marsh, D. R., Mills, M., Alterskjaer, K., Muri,

Atmos. Chem. Phys. Discuss., https://doi.org/10.5194/acp-2018-141
Manuscript under review for journal Atmos. Chem. Phys.
Discussion started: 15 February 2018

H., Kristjánsson, J. E., Boucher, O., Schulz, M., Cole, J. N. S., Curry, C. L., Jones, A., Haywood, J., Irvine, P. J., Ji, D., Moore, J. C., Karam, D. B., Kravitz, B., Rasch, P. J., Singh, B., Yoon, J.-H., Niemeier, U., Schmidt, H., Robock, A., Yang, S., and Watanabe, S.: The hydrological impact of geoengineering in the Geoengineering Model Intercomparison Project (GeoMIP), Journal of Geophysical Research: Atmospheres, 118, 11,036-011,058, 10.1002/jgrd.50868, 2013.

Tokinaga, H., Xie, S. P., Deser, C., Kosaka, Y., and Okumura, Y. M.: Slowdown of the Walker circulation driven by tropical Indo-Pacific warming, Nature, 491, 439-443, 2012.

Vallis, G. K., Zurita-Gotor, P., Cairns, C., and Kidston, J.: Response of the large-scale structure of the atmosphere to global warming, Q J Roy Meteor Soc, 141, 1479-1501, 2015.

Van der Wiel, K., Matthews, A. J., Joshi, M. M., and Stevens, D. P.: Why the South Pacific Convergence Zone is diagonal, Clim Dynam, 46, 1683-1698, 2016.

Vecchi, G. A., Soden, B. J., Wittenberg, A. T., Held, I. M., Leetmaa, A., and Harrison, M. J.: Weakening of tropical Pacific atmospheric circulation due to anthropogenic forcing, Nature, 441, 73-76, 2006.

Vecchi, G. A., and Soden, B. J.: Global warming and the weakening of the tropical circulation, J Climate, 20, 4316-4340, 2007.

Watanabe, S., Hajima, T., Sudo, K., Nagashima, T., Takemura, T., Okajima, H.,

Atmos. Chem. Phys. Discuss., https://doi.org/10.5194/acp-2018-141
Manuscript under review for journal Atmos. Chem. Phys.
Discussion started: 15 February 2018

Nozawa, T., Kawase, H., Abe, M., Yokohata, T., Ise, T., Sato, H., Kato, E., Takata, K., Emori, S., and Kawamiya, M.: MIROC-ESM 2010: model description and basic results of CMIP5-20c3m experiments, Geosci Model Dev, 4, 845-872, 2011.

Waugh, D. W., Garfinkel, C. I., and Polvani, L. M.: Drivers of the Recent Tropical Expansion in the Southern Hemisphere: Changing SSTs or Ozone Depletion?, J Climate, 28, 6581-6586, 2015.

FIGURES

Atmos. Chem. Phys. Discuss., https://doi.org/10.5194/acp-2018-141
Manuscript under review for journal Atmos. Chem. Phys.
Discussion started: 15 February 2018

Atmospheric Chemistry and Physics
Open Access
Discussions

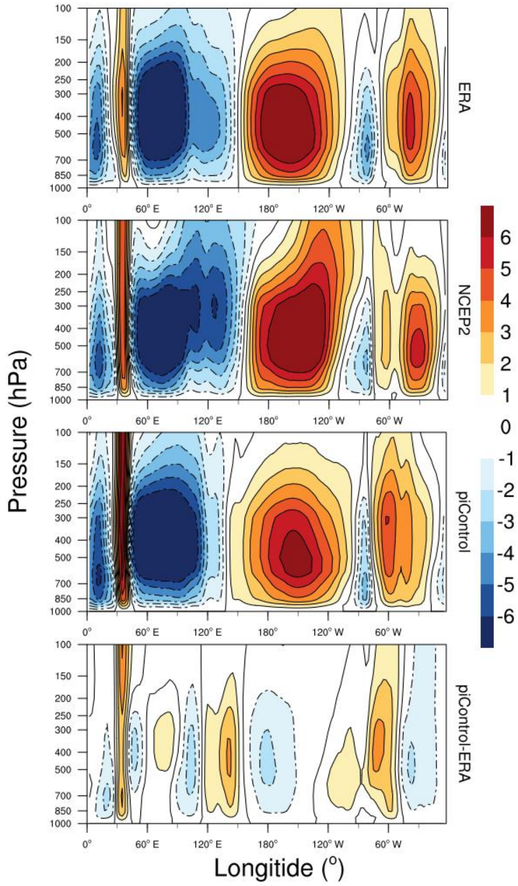

Figure 1. The ERA-Interim reanalysis (top), NCEP2 reanalysis (second row), model ensemble mean Walker circulation under piControl (third row) and difference between ERA-Interim and piControl (bottom). Color bar indicates the value of averaged zonal mass stream-function (10^{10} kg s^{-1}). Warm color (positive values) indicate a clockwise rotation and cold color (negative values) indicate an anticlockwise rotation.

Atmos. Chem. Phys. Discuss., https://doi.org/10.5194/acp-2018-141
Manuscript under review for journal Atmos. Chem. Phys.
Discussion started: 15 February 2018

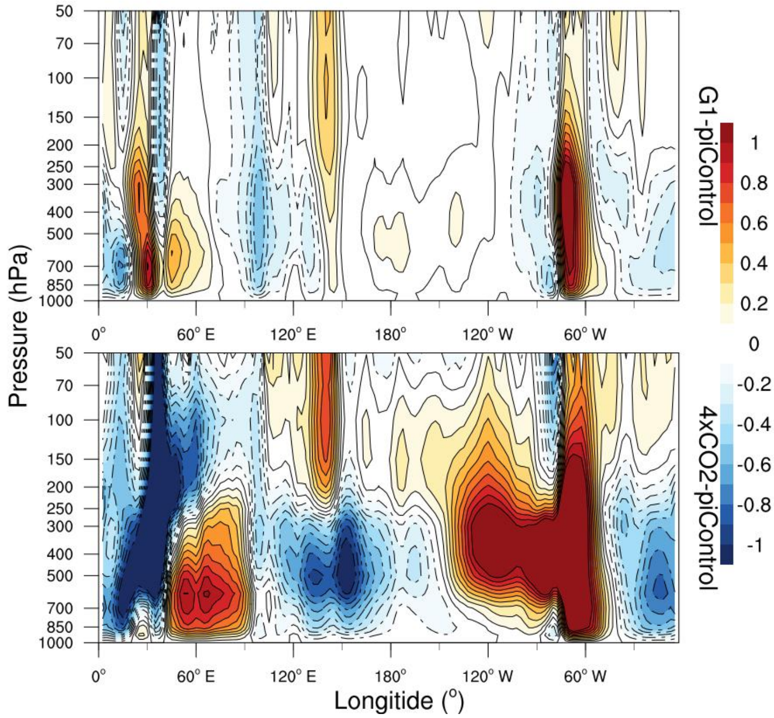

Figure 2. Same as Fig. 1. But the top and bottom respectively indicate the anomalies relative to piControl for G1 and abrupt4×CO_2 experiments.

Atmos. Chem. Phys. Discuss., https://doi.org/10.5194/acp-2018-141
Manuscript under review for journal Atmos. Chem. Phys.
Discussion started: 15 February 2018

Atmospheric Chemistry and Physics
Open Access
Discussions

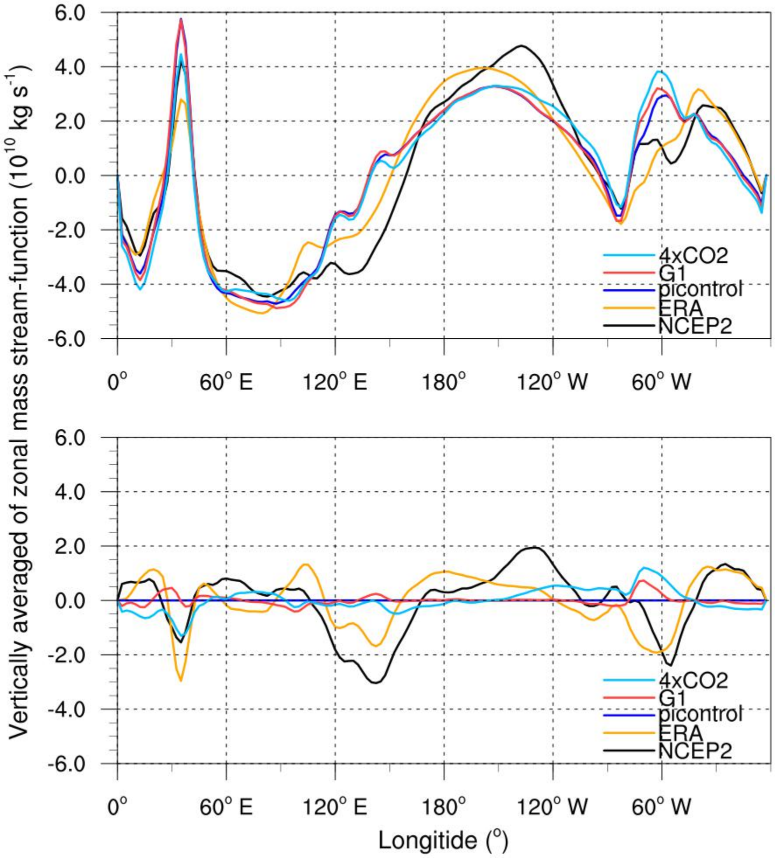

Figure 3. The vertically averaged zonal mass stream-function (10^{10} kg s^{-1}) in piControl, G1, abrupt4×CO2 experiment for ensemble mean, ERA-Interim and NCEP2 are in the top panel. Lines in bottom panel are the difference between piControl and other scenarios.

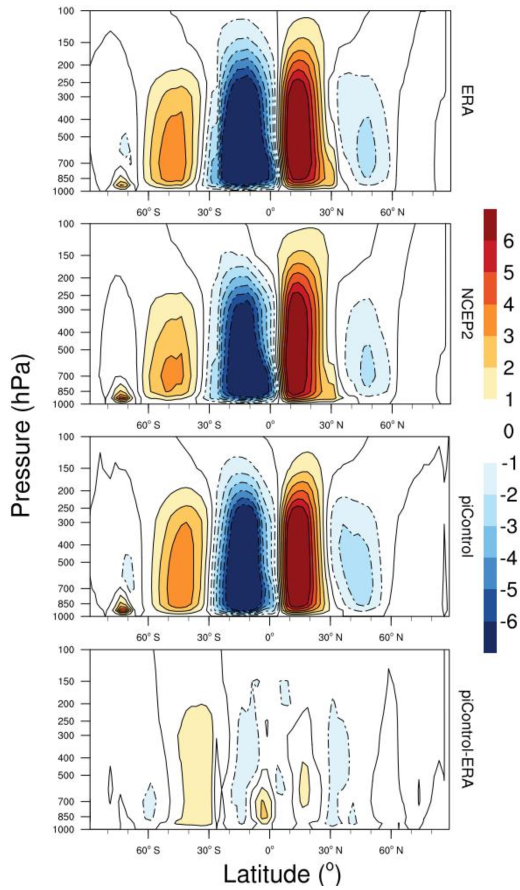

Figure 4. The ERA-Interim reanalysis (top), NCEP2 reanalysis (second row), model ensemble mean Hadley circulation under piControl (third row) and difference between ERA-Interim and piControl (bottom). Color bar indicates the value of averaged meridional mass stream-function (10^{10} kg s^{-1}). Warm colors (positive values) indicate a clockwise rotation and cold colors (negative values) indicate an anticlockwise rotation.

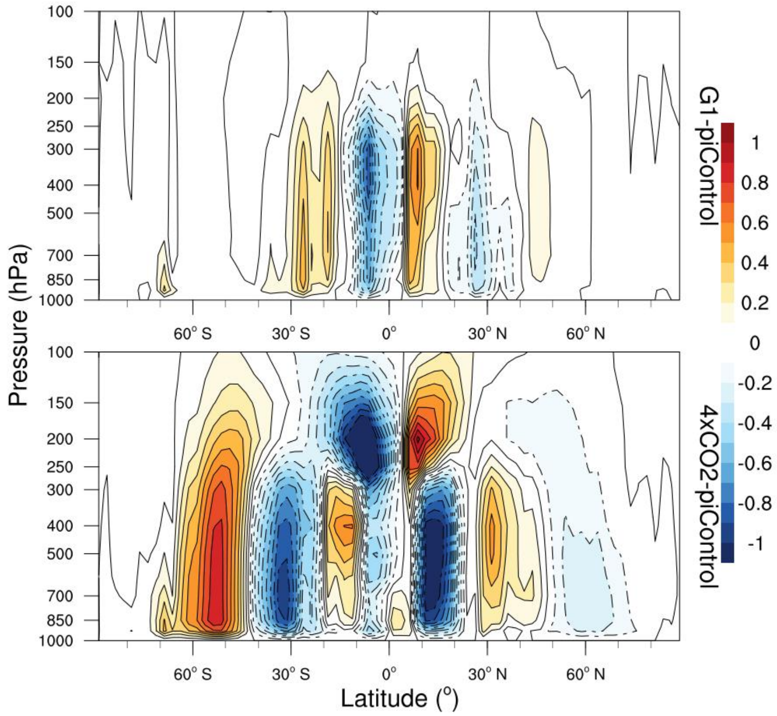

Figure 5. Model ensemble mean meridional stream-function anomalies G1-piControl (top) and abrupt4×CO_2-piControl (bottom). Contours and color bar indicate the value of averaged meridional mass stream-function (10^{10}kg s^{-1}).

Atmos. Chem. Phys. Discuss., https://doi.org/10.5194/acp-2018-141
Manuscript under review for journal Atmos. Chem. Phys.
Discussion started: 15 February 2018

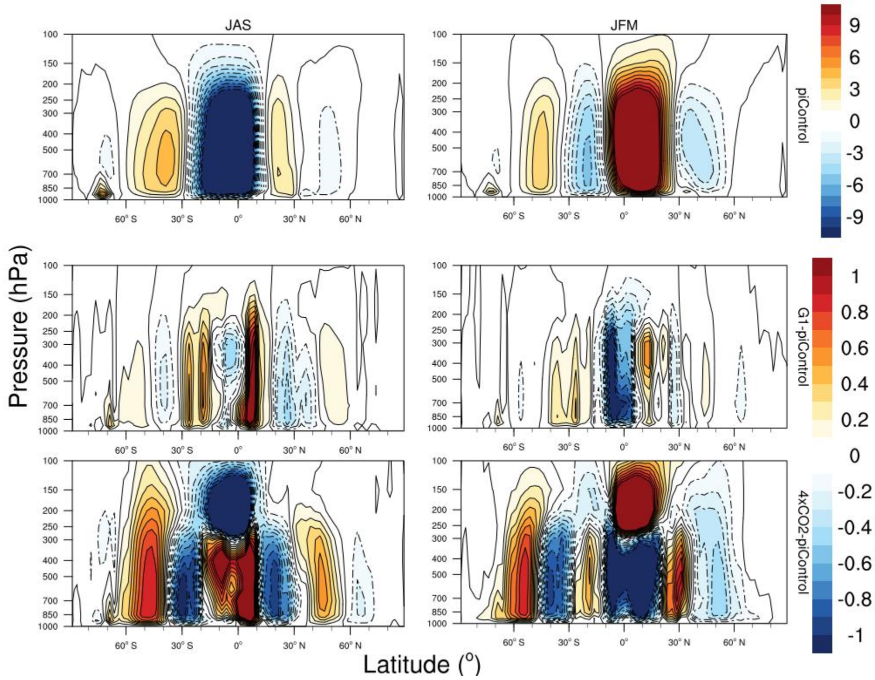

784

785 **Figure 6.** Model ensemble mean meridional stream-function in JAS (left) and JFM
786 (right). Top shows piControl, while center and bottom row respectively indicate the
787 anomalies relative to piControl for G1 and abrupt4×CO_2 experiments. Color bar
788 indicates the value of averaged meridional mass stream-function (10^{10} kg s^{-1}). Warm
789 colors (positive values) indicate a clockwise rotation and cold colors (negative values)
790 indicate an anticlockwise rotation.

791

Atmospheric Chemistry and Physics
Open Access
Discussions
EGU

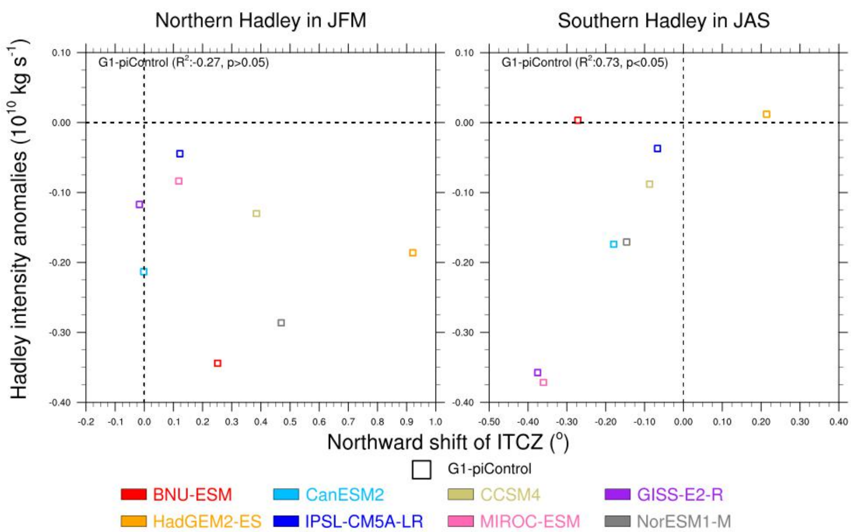

Figure 7. Change of Hadley cell intensity as a function of ITCZ position under G1 relative to piControl across the models. The ITCZ position is defined from the centroid of precipitation (Smyth et al., 2017).

Atmos. Chem. Phys. Discuss., https://doi.org/10.5194/acp-2018-141
Manuscript under review for journal Atmos. Chem. Phys.
Discussion started: 15 February 2018

Atmospheric Chemistry and Physics
Open Access
Discussions

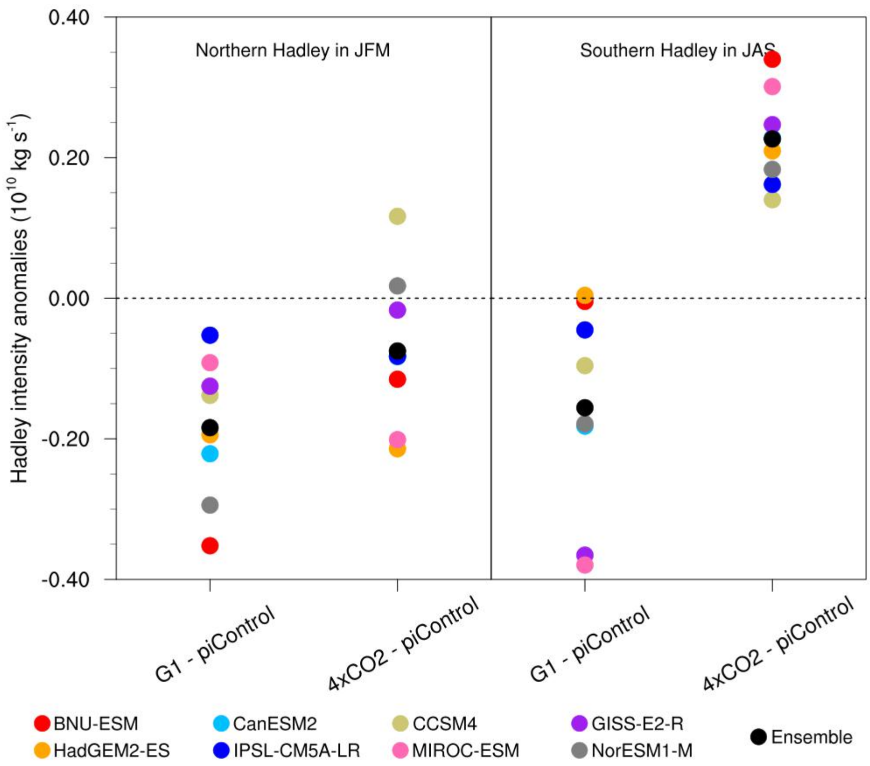

Figure 8. Anomalies (10^{10} kg s^{-1}) amongst models in Hadley circulation for the southern cell in JAS (left panel), defined as the magnitude of the mean meridional stream-function between 15°N and 40°S, and (right panel) the northern cell in JFM, defined as the magnitude of the mean meridional stream-function between 15°S and 40°N. The dot size for the models is about 1 standard error of the model mean.

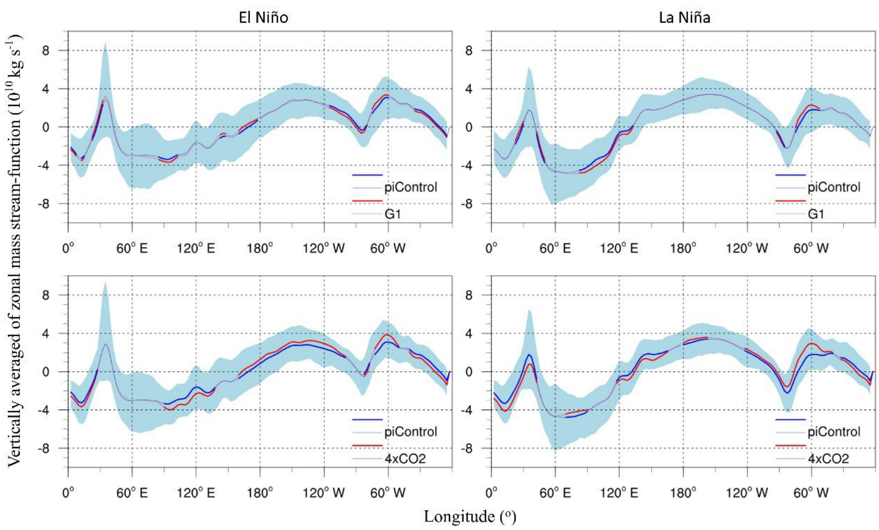

Figure 9. The vertically averaged of zonal mass stream-function under ENSO. For El Niño or La Niña conditions, blue line in each panel represent the vertically averaged of zonal mass stream-function (10^{10} kg s^{-1}) under piControl. Red line in top row is G1 and bottom row abrupt4×CO2. Thick lines denote locations where circulation changes are significant at the 95% confidence level. The 16%-84% range across the 8 individual models are show by light blue shading.

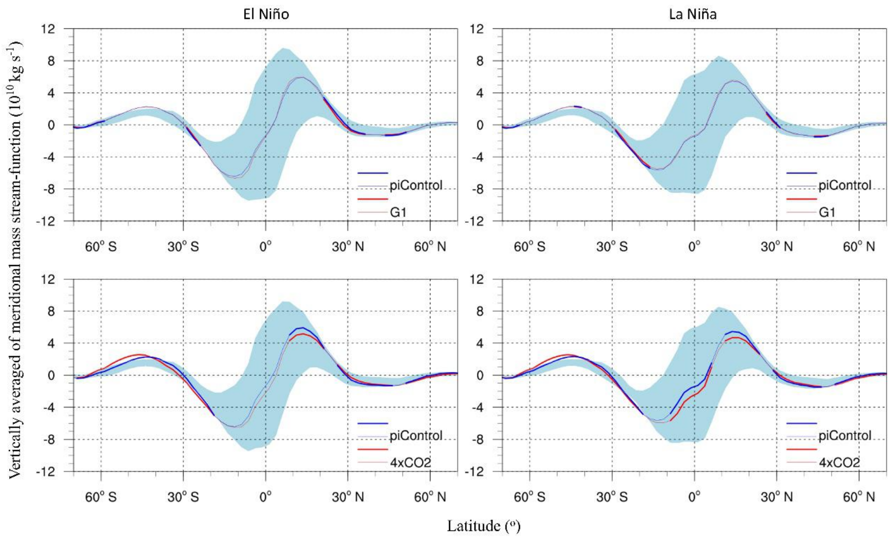

Figure 10. The vertically averaged of meridional mass stream-function under ENSO. For El Niño or La Niña conditions, blue line in each panel represent the vertically averaged of zonal mass stream-function (10^{10} kg s^{-1}) under piControl. Red line in top row is G1 and bottom row abrupt4×CO_2. Thick lines denote locations where circulation changes are significant at the 95% confidence level. The 16%-84% range across the 8 individual models are show by light blue shading.

Atmos. Chem. Phys. Discuss., https://doi.org/10.5194/acp-2018-141
Manuscript under review for journal Atmos. Chem. Phys.
Discussion started: 15 February 2018

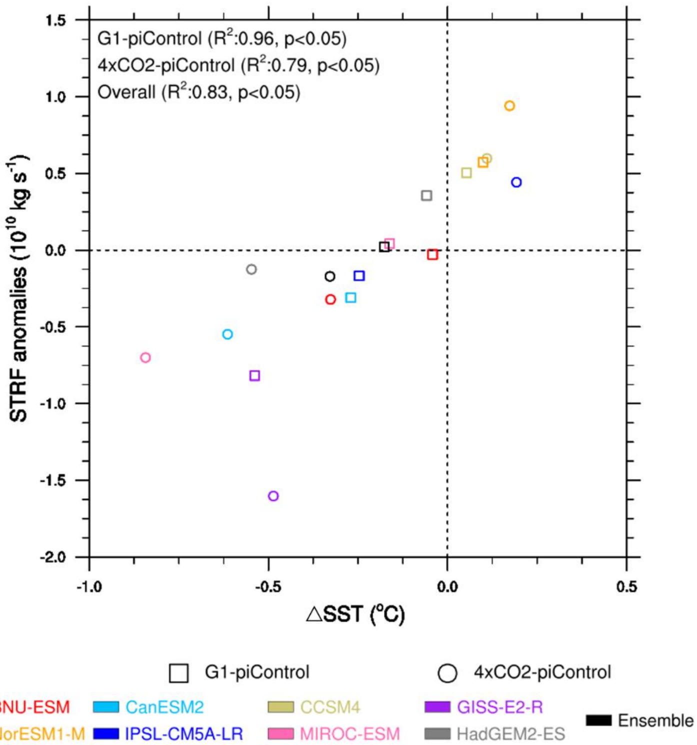

Figure 11. Model mean monthly anomalies relative to each model's piControl of STRF and ΔSST. Positive value of STRF and ΔSST indicate strengthening of the Walker circulation.

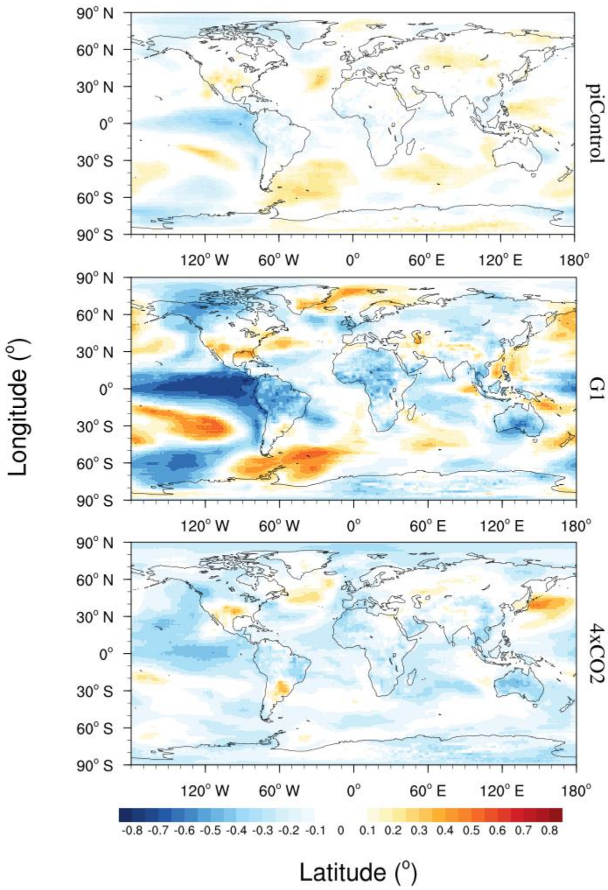

Figure 12. Mean correlation between yearly STRF and global gridded 2 m temperatures for 100 years of piControl (top row), and the final 30 years of G1 (middle row) and abrupt4×CO_2 (bottom row) experiments for 8 models ensemble mean.

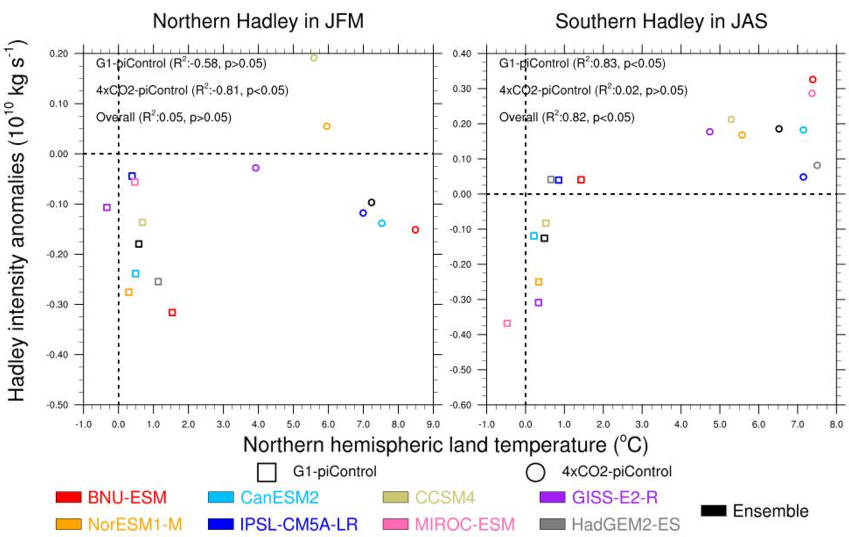

Figure 13. Hadley intensity mean model anomalies versus the northern hemisphere land temperature for the northern Hadley cell (left) in JFM and the southern Hadley cell in JAS (right). Positive value of Hadley intensity indicates Hadley circulation strengthening regardless of the direction.

Table 1. The GeoMIP, CMIP5 models and reanalysis data used in the paper

No.	Model[1]	Reference	Lat × Lon
1	BNU-ESM	Ji et al. (2014)	2.8°×2.8°
2	CanESM2	Arora et al. (2011)	2.8°×2.8°
3	CCSM4	Gent et al. (2011)	0.9°×1.25°
4	GISS-E2-R	Schmidt et al. (2014)	2°×2.5°

Atmos. Chem. Phys. Discuss., https://doi.org/10.5194/acp-2018-141
Manuscript under review for journal Atmos. Chem. Phys.
Discussion started: 15 February 2018

5	HadGEM2-ES	Collins et al. (2011)	1.25°×1.875°
6	IPSL-CM5A-LR	Dufresne et al. (2013)	2.5°×3.75°
7	MIROC-ESM	Watanabe et al. (2011)	2.8°×2.8°
8	NorESM1-M	Bentsen et al. (2013), Iversen et al. (2013)	1.9°×2.5°
9	NCEP-DOE (NCEP2)	Kanamitsu et al. (2002)	2.5°×2.5°
10	ERA-Interim	Simmons et al. (2007)	0.75°×0.75°

1. Full Names: BNU-ESM, Beijing Normal University-Earth System Model; CanESM2, The Second Generation Canadian Earth System Model; CCSM4, The Community Climate System Model Version 4; GISS-E2-R, Goddard Institute for Space Studies ModelE version 2; IPSL-CM5A-LR, Institut Pierre Simon Laplace ESM; MIROC-ESM, Model for Interdisciplinary Research on Climate-Earth System Model; NorESM1-M, Norwegian ESM.

Table 2. The change of Walker circulation position (°) and intensity (10^{10} kg s^{-1}) in 8 models and their ensemble mean. The number in the brackets represent percentage change relative to piControl. Negative position (STRF) represent westward movement (weakening) and positive value represent eastward movement (strengthening). Statistically significant differences at the 5% are in shown in bold.

Earth System Model	G1	abrupt4×CO_2

	Position	STRF	Position	STRF
BNU-ESM	0.32(0.2)	-0.04(-2.3)	**8.6(5.8)**	**-0.34(-18)**
CanESM2	**3.8(2.7)**	**-0.32(-11)**	**16.4(11.5)**	**-0.56(-19.3)**
CCSM4	-1(-0.7)	**0.5(20.6)**	-0.3(-0.2)	**0.58(24.6)**
GISS-E2-R	**10.6(6.5)**	**-0.83(-73.5)**	**21.2(13)**	**-1.6(-142.7)**
HadGEM2-ES	-1(-0.7)	**0.34(10.8)**	**4.9(3.3)**	**-0.14(-4.4)**
IPSL-CM5A-LR	1.4(1)	**-1.8(-7.8)**	0.15(0.1)	**0.43(18.3)**
MIROC-ESM	0.5(0.4)	0.03(0.7)	**-5.2(-4.2)**	**-0.72(-19.1)**
NorESM1-M	**-3.7(-2.3)**	**0.56(20.2)**	**-6.6(-4.2)**	**0.93(33.6)**
Ensemble	-0.5(-0.3)	0.007(0.3)	**4(2.8)**	**-0.19(-7.1)**

Table 3. The percentage changes in G1-piControl and abrupt4×CO_2-piControl relative to piControl in a 4 model (BNU-ESM, IPSL-CM5A-LR, HadGEM2-ES, MIROC-ESM) ensemble mean. Functions 1 and 2 are scale factors for Hadley circulation (Seo et al., 2014). Function 1 is $\frac{5}{2}\frac{\delta H}{H}+\frac{5}{2}\frac{\delta \Delta_H}{\Delta_H}-\frac{\delta \Delta_V}{\Delta_V}$ and is based the model of Held and Hou (1980), while function 2 is $\frac{9}{4}\frac{\delta H}{H}+2\frac{\delta \Delta_H}{\Delta_H}-\frac{3}{4}\frac{\delta \Delta_V}{\Delta_V}$ which is derived from the model by Held (2000). Δ_H is meridional temperature gradient defined as $\frac{\theta_{eq}-\theta_{higher\ lat}}{\theta_0}$ which is the tropospheric mean meridional potential temperature gradient with θ_0 denoting the hemispheric troposphere mean potential temperature and θ_{eq}

Atmos. Chem. Phys. Discuss., https://doi.org/10.5194/acp-2018-141
Manuscript under review for journal Atmos. Chem. Phys.
Discussion started: 15 February 2018

Atmospheric Chemistry and Physics Discussions

calculated between 10°N and 10°S. We follow Seo et al. (2014) in taking $\theta_{higher\,lat}$ as the average potential temperature between 10°-50°N for the northern hemisphere winter and 10°-30°S for the southern hemisphere. $\Delta_V = \frac{\theta_{300} - \theta_{925}}{\theta_0}$ is the dry static stability of the tropical troposphere. H is the tropical tropopause height estimated as the level where the lapse rate decreases to 2°C km^{-1}. The Hadley intensity ψ_m is described in section 2.3.

Scenario	G1-piControl		abrupt4×CO_2-piControl	
	North	South	North	South
Temperature gradient	-2.6	-1.2	-4.4	-4
Static stability	-3.4	-3.2	21	23
Subtropical tropopause height	-0.1	-0.5	0.87	3
Function 1	-3.35	-1.05	-29.8	-25.5
Function 2	-2.9	-1.13	-22.6	-18.5
Hadley intensity	-3.7	-1.2	-3.4	4.3